Influence of deep foundations in a deck slab high-speed railway bridge: A theoretical study

Influencia de las cimentaciones profundas en la losa de tablero de un puente ferroviario de alta velocidad: un estudio teórico

A. M. de la Concha[a], D. Suescum-Morales[b], M. Martínez Sánchez[a] y H. Cifuentes[a,*]

[a] 1School of Engineering, Department of Continuum Mechanics and Structural Analysis, University of Seville.
bSchool of Civil Engineering, Construction Engineering Area, University of Cordoba.
*Corresponding author: School of Engineering, Department of Continuum Mechanics and Structural Analysis, University of Seville.

ABSTRACT

In this research, the importance of properly modeling the infrastructure of high-speed railway bridges with deep foundations when using the finite element method (FEM) is discussed. To do so, an isolated deck and several complete models with different characteristics were compared. Parameters such as the length of the piles, the stiffness of the supporting layers and the type of dynamic load (10 different trains) were explored. This study started with the analysis of various parameters that determine the behavior of deep foundations with piles in simplified models. Based on these findings, a complete model was built. This research shows the importance of including not only the surrounding terrain but also the main substructure (i.e., piers and abutments) in the model. Recommendations on the amount of soil to include, its mechanical properties and the length of the piles needed are also provided to ensure the reliability of results when considering the soil-structure dynamic interaction. With this research, a contribution to current knowledge is intended through a series of guidelines and tools to help structural engineers in dynamic simulations through a theoretical case study.

KEYWORDS: Dynamic analysis, high-speed trains, railway bridges, soil-structure interaction, pile foundation, infrastructure, numerical simulations.

RESUMEN

En esta investigación se discute la importancia de modelizar adecuadamente la infraestructura de los puentes ferroviarios de alta velocidad con cimentaciones profundas cuando se utiliza el método de elementos finitos (FEM). Para ello, comparamos la respuesta de un tablero aislado y varios modelos de puentes completos con modelos de terrenos de diferentes características. Se exploran parámetros como la longitud de los pilotes, la rigidez de las capas de soporte y el tipo de carga dinámica (10 trenes diferentes). Este estudio comienza con el análisis de varios parámetros que determinan el comportamiento de las cimentaciones profundas con pilotes en modelos simplificados. Basándonos en estos hallazgos, se construyen los modelos completos. Esta investigación muestra la importancia de incluir no solo el terreno circundante, sino también la subestructura principal (es decir, pilares y estribos) en el modelo. También se proporcionan recomendaciones sobre la cantidad de suelo a incluir, sus propiedades mecánicas y la longitud de los pilotes necesarios para garantizar la fiabilidad de los resultados al considerar la interacción dinámica suelo-estructura. Con esta investigación, pretendemos contribuir al conocimiento actual con una serie de directrices y herramientas para ayudar a los ingenieros estructurales en simulaciones dinámicas a través de un estudio de caso teórico.

PALABRAS CLAVE: Análisis dinámico, trenes de alta velocidad, puentes de ferrocarril, interacción suelo-estructura, cimentaciones profundas, infraestructura, simulaciones numéricas.

* Persona de contacto / *Corresponding author*:
 Correo-e / *e-mail*: delaconcha@us.es (Antonio Martínez de la Concha)

1.
INTRODUCTION

High-speed railways have requirements for bridges due to the dynamic loads associated to train traffic. Considering this, the study of the dynamic behavior of railway bridges has become a key factor in the design of such structures [1–5]. The stresses and strains observed in a railway bridge due to train traffic can exceed the design limits (i.e., targets), particularly if the frequency of the applied loads matches the natural frequency of the structure as a result of undesired resonance. This is why the natural frequency of the structure should be tuned away from the frequency of the loads, as explained by Shen-Haw (2003) [6]. This phenomenon can lead to the inoperability of the structure and, in extreme cases, to its collapse.

The growth of the construction of high-speed railways has increased the concern and awareness of traffic-induced vibrations among engineers and scientists [7,8]. This has led to impose limits on maximum accelerations and deflections using different codes and to prescribe an impact factor that is used to scale up the static loads in an effort to capture the dynamic effects [9,10]. Dynamic simulations that are often conducted with time-consuming finite element methods (FEM) have become essential for avoiding such problems. Therefore, guidelines and tools to assist structural engineers in the process are needed [11].

Hence, capturing the behavior of the structure in a realistic manner is very important. In this regard, the development of computational methods has resulted in great progress in terms of knowledge and accuracy of analysis [12–14]. Some models take into account not only the motion of the loads on the bridge, but also changes in their magnitudes due to the dynamic interaction between the structure and the train suspension [15–17].

The dynamic loads used in this paper follow those proposed by the European design code [9], which are based on the High-Speed Load Model (HSLM) and comprise a series of fictitious trains proposed by ERRI D214 [8]. The loads are constant in magnitude for a given axle and move along the structure following the train motion. These load recommendations can also be found in other codes such as IAPF-07 [10]. It is not possible to conduct an analysis including multibody behavior because each train is composed of the car body, bogie, wheelset, primary and secondary suspension, axle box, yaw damper, lateral damper, antirolling torsion bar, rotating arm, lateral stop and traction rod [18,19]. This study focused on the envelope behavior of the potential traffic over the bridge, as is usual in codes.

As discussed in Martínez De la Concha et al. [20], most models only include the structure and disregard the supporting terrain by applying displacement boundary conditions directly on the structure. The simple linear elastic beams or frame structure are often used to simulate the vehicle-bridge dynamic response [21]. This simplification reduces the computational cost but assumes that the soil has infinite stiffness, as pointed out by Zangeneh et al. (2018) [22].

Limited material has been published regarding the influence of the soil-structure interaction (SSI) on the behavior of high-speed railway bridges. There are even fewer studies

that also cover deep foundation models (i.e., with piles). An example is the study by Takemiya (2007) [23], which explored the behavior of high-speed railway structures and the surrounding terrain in Japan through the23 FEM. It concluded that including the soil-structure interaction was crucial to properly capture the behavior of the structure. Mahir Ülker-Kaustell had similar findings in his simplified analysis of a portal frame railway bridge [24]. Not including the supporting soil in the model can decrease the damping of the model, increasing the magnitude of displacements during resonance [25,26]. The boundary element method (BEM) has a great application in the study of the soil-structure interaction [27,28], allowing for more accurate analysis. It also eliminates the need to define an external contour in the model and has been used for longer than the FEM in this field [29]. Nevertheless, the FEM was chosen because it is widely used in the study of these structures. The BEM is less common in practical applications.

No references to previous studies that explored the SSI as well as the influence of the following parameters were found: (i) different soil stiffness; (ii) different soil depth (i.e., different depths of piles); (iii) a speed sweep from 20 km/h to 420 km/h; and (iv) using 10 trains with different wheel-bases and loads per axle. Following the formulation used in a recent study [20], two analyses methods were used: direct integration analysis of the complete model using the Newmark method in Abaqus (Abaqus/standard, version 6.14), and modal superposition analysis using SAP2000. For the direct integration analysis of the complete model, an amplitude decay factor of $\gamma = 0.005$ was used. Abaqus 6.14 and SAP2000 v14 software were used, as they are among the most commonly used tools for this type of study. [30–33].

The main novelty from the previous research by Martínez-De la Concha et al. [20], was the study of deep foundations. Regarding this particular issue, all the parameters to build the model including the infrastructure were new. The aim of this theoretical study with the FEM was to compare the results of the dynamic impact coefficient from a model that does not include the infrastructure (e.g., surrounding soil, piers, abutment and pile foundation) to a model that includes it. Parameters such as the length of the piles, the stiffness of the supporting layers, and the type of dynamic load (i.e., 10 different trains) were explored.

This study began with the analysis of various parameters that control the behavior of deep foundations with piles in simplified models. Based on these findings, a complete model was built. A contribution to current knowledge is intended through a series of guidelines and tools to assist structural engineers in dynamic simulations, using a theoretical case study.

2.
MODEL DESCRIPTION

2.1. Simplified foundation model

The objective of these analyses was to identify and tune the parameters that control the behavior of a deep foundation
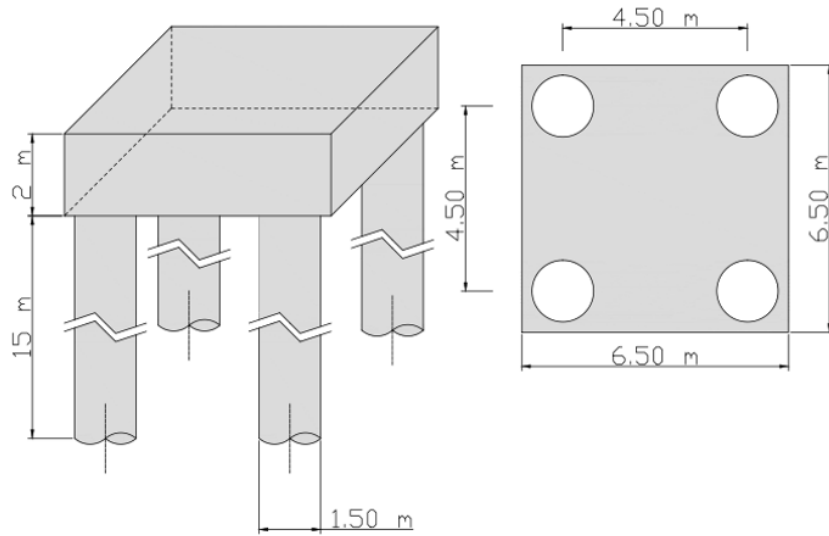
Figure 1. Model of pile cap for the simplified foundation model.

model (i.e., piles and pile cap) to ensure reliable converged results. Parameters such as finite element size and type, pulse duration, and the amount of soil to be included were considered. For this study, several simplified models were developed in which the influence of these parameters on the response was analyzed. Based on the results, a complete model was subsequently built. In the first simplified model, the response of a square pile cap (6.5 × 6.5 × 2.0 meters) was analyzed. The pile cap was supported on 4 circular piles with a length of 15 m and a diameter of 1.5 m (Figure 1).

The model included a portion of soil around the piles whose dimensions and characteristics were parameters to be studied. The piles and pile cap had the following mechanical characteristics: elastic modulus E=30 GPa, Poisson coefficient γ= 0.2 and a specific concrete weight of γ_c = 25 kN/m³. Two soil layers were considered: a 7 m meter deep superficial layer with softer properties (E = 3 MPa, v = 0.35 and a specific soil weight of γ_s = 20 kN / m³); and a stiffer material layer underneath (E = 30 MPa, = 0.35 and a specific soil weight of γ_s = 20 kN / m³). A relatively low stiffness material was still used, since the behavior of the system was intended to be analyzed on a deformable elastic bed [34]. Five percent of the critical damping was used in the soil material definition [34,35].

In the five faces defined by the soil boundary included, (every face unless top face) normal displacements were constrained. There was no relative movement in the concrete-soil interface. Instead, both meshes moved together like a continuous mesh. For this foundation model, three sensitivity studies were carried out:

(1) finite element size;
(2) pulse duration; and
(3) volume of soil included in the model.

All model components were discretized using C3D4-type elements from the Abaqus library, that is, first-order tetrahedral elements. The models were run using direct integration in Abaqus/Explicit with the default values for numerical damp-

ing (i.e., a linear bulk viscosity of 0.06 and a quadratic bulk viscosity of 1.2). Since the same level of accuracy was not required in the entire modeled domain, local mesh refinements were applied where higher accuracy was needed. It is important to consider the effects on wave propagation when meshing the different models.

To identify the requirements for element size, the smallest model (Model 1 on Table 1) was meshed with three different element sizes – 30, 40 and 50 cm –, resulting in models with 43,469, 21,535 and 12,772 degrees of freedom respectively. A uniform pressure load was applied on the pile cap upper face. Its magnitude was time-dependent following triangular amplitude. The response was analyzed against two different loads: a short pulse of 1 MPa maximum pressure and a duration of 10 ms; and a long pulse of 20 kPa of peak pressure and a duration of 500 ms. In both cases, the magnitude of the pulse was the same. The first one aimed to highlight the behavior during higher frequency dynamic events while the second one assessed loads that better represent the typical dynamic loads produced by train traffic. This statement follows Frýba (1996) [36].

To identify the amount of soil to include in the FEM model, it was necessary to explore it to maintain result accuracy while keeping the computation cost down. Simpler theoretical models, which can be solved analytically assuming isotropic and homogeneous linear elastic properties, consider the soil as a homogeneous half-space. Such is the case of studies conducted with the boundary element method (BEM) [37]. Hence, our models had the same conditions.

Pile cap width (6.5 m) was adopted as the characteristic length in the model. Five models with different amounts of soil were analyzed. The size of the models was the result of adding 6.5 m of soil around the pile cap and also 6.5 m of soil under the pile toe line. Subsequent models were built by adding 6.5 m of soil in each direction to the previous model. Additionally, a model with a very large portion of soil (i.e., the Limit model) was analyzed to verify that the reflection
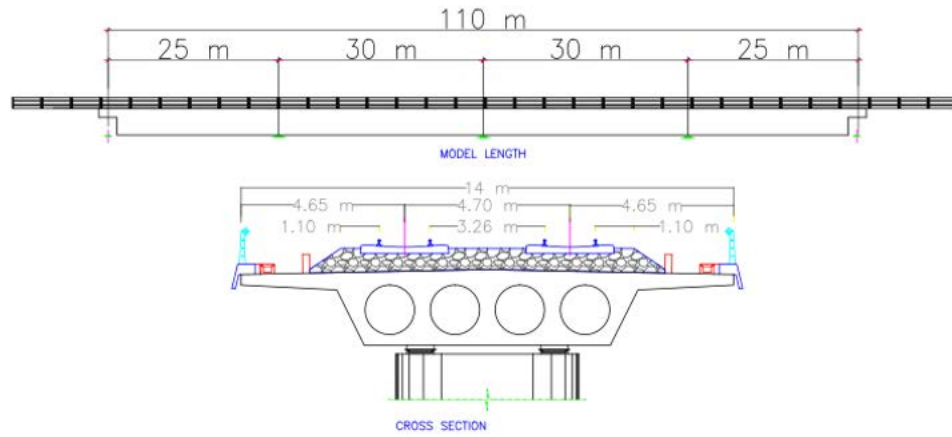
Figure. 2. Geometric description of the isolated deck model.

of waves in the boundary did not interfere with the simulation results meaningfully. To this end, the soil contours were moved out far enough so that the P waves had no time to reflect and return in the simulated time interval [22]. Table 1 presents the dimensions of the models described above.

TABLE 1.
Simplified foundation model dimensions

Model name	Dimensions (m)			Soil under the end pile
	X	Y	Z	
Model 1	19.5	19.5	23.5	6.5
Model 2	32.5	32.5	30	13
Model 3	45.5	45.5	36.5	19.5
Model 4	58.5	58.5	43	26
Limit model	162.5	162.5	95	78

2.2. Bridge models

To analyze the bridge structure, two models were built: one including infrastructure and one excluding it. Those models were studied using a specific bridge software package: SAP2000 v14. Both models were explored using both modal superposition and direct integration. Sometimes the model includes elements such as the abutments and/or piles, but it rarely includes the soil-structure interaction [38]. Bridges are typically analyzed with models that only consider their deck [36]. The aim of our models was to assess the impact of the previous simplification. This required assessing the behavior of a simply supported isolated deck so that it could be compared with a complete one, which included the infrastructure.

2.2.1. Isolated deck model

The deck of the bridge studied in this paper was identical to the one analyzed by the authors in previous research [20]. Its main characteristics are described below. In this model, we assumed displacement boundary conditions assuming infinitely stiff piers and abutments [14]. Shell elements with both membrane and plate degrees of freedoms were used. Flexural (i.e., plate) behavior considers rotational stiffness along the two axes in the

element plane as well the displacement in the normal direction (i.e., Kirchoff's formulation) [32]. For the membrane behavior, we used an isoparametric formulation that included the translational degrees of freedom in the element plane as well as the rotation within it. Displacements in the element plane were considered using quadratic shape functions, and out-of-plane displacements were considered with cubic functions.

The modeled bridge had 4 spans so that the model included the interaction between spans accurately enough with an affordable computational cost. The bridge had two 30-m-long spans in the middle and one 25-m-long span at either end. The deck cross section was a 2.00-m-thick lightened slab with four 1.4-m-diameter circular lightening holes (Figure. 2). The slab was 14.00 m wide, which is standard for a double track line in Spain [39].

The location of the nodes in the cross section is shown in Figure 3. The thickness of the elements was adjusted to obtain a section with the same area (i.e., same mass) as the real deck. A 1 m element size was used in the cross section and matched the element size along the bridge, resulting in approximately square elements as shown in Figure 3.
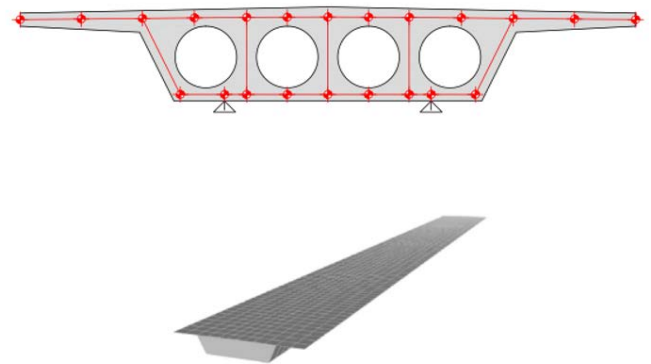

Figure. 3. Schematic view of the model cross section and mesh discretization of the isolated deck.

Elements in the deck cross section were added on top of the abutments and piles to model the diaphragms. To visualize this, the elements modeling the webs and the bottom slab were concealed in Figure 4.
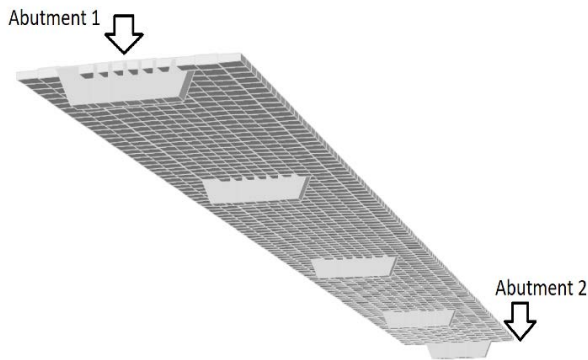
Figure. 4. Diaphragm modeling detailed view.

The masses corresponding to the permanent loads were distributed over the upper slab. The permanent loads attributed to each element were as follows (kN/m): 94.84 (ballast); 6.70 (sleepers); 1.18 (rails); 5 (small wall); 3.78 (troughs); 9.59 (barrier rail) and 1.02 (railings).

The vertical displacement in all support points (Figure 3) was constrained. The lateral motion was constrained in one support location per pier/abutment. Finally, the longitudinal displacement was constrained in both support nodes only at one end of the bridge (Abutment 1). The mechanical properties of the deck were as follows: elastic modulus (E) 30 GPa; Poisson coefficient $v = 0.2$ specific weight $\rho = 25$ kN/m³; and damping ξ 3%.

Universal dynamic A train loads, also known as High-Speed Load Model (HSLM) loads, were applied. They consist of 10 trains with different wheelbases and loads per axle in various configurations [8]. These are the dynamic loads recommended by the main regulations for the design of new railway lines [9,10]. Following the standards [10], a 350 km/h design speed was considered and, consequently, a speed sweep was analyzed from 20 km/h to 420 km/h (i.e., 1.2 times the design speed) with a 10 km/h step.

The traffic load was distributed among the nodes under the railway in the cross section. The applied force on each node was proportional to the surface of the sleeper over it (Figure 5). It was assumed that the load propagates uniformly with a 1/4 slope through the ballast and the sleeper distributes the load uniformly. This load application procedure is described in the Spanish code for this type of structures [10].
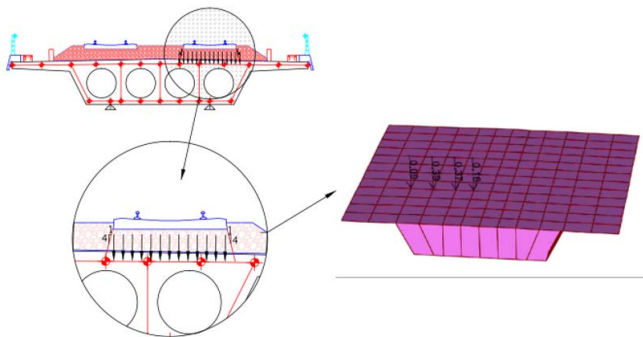

Figure 5. Load modeling in the cross section for the isolated deck model and complete model.

In the longitudinal direction, the load was distributed in a linear fashion among two consecutive sections based on the distance between the load and the section at that particular time. This resulted in a series of triangular history loads as the different axles of the train traveled over a specific cross section of the bridge (Figure 6).
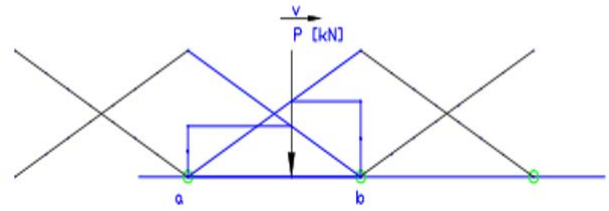

Figure 6. Longitudinal load distribution.

The study focused on the central section of the bridge, specifically on the node of the upper slab that is centered with the track where the time-history loads are applied. This node captures the displacements of the track supports and ultimately of the trains that travel on top of them. The maximum vertical displacement observed in this node during the entire simulation was compared.

Dynamic amplification is captured by the impact factor (Φ), a commonly used parameter [8,10] that normalizes the maximum deflection observed among all trains and across all speeds with that of the UIC-71 train [9] statically. For this paper and following the results of previous research [20], a different definition of the impact factor was used. Instead of using the UIC-71 train, each train dynamic response was normalized with its own static deflection.

2.2.2. Complete model of the railway bridge

In this section, the soil-structure interaction was introduced into models with deep foundations. The model used in this section consisted of a deck that was identical to that described in Section 2.2, both geometrically and regarding loads. That deck was supported by 10-m-high abutments and 3 piers. The outboard piers were 20 m high while the pier at the center of the bridge measured 25 m. The abutments were of the closed type and consisted of a 1.00-m-thick and 10-m-high front wall with two lateral walls (i.e., wing walls) that were also 1.00 m thick. The abutment foundations were pile caps (14.00 x 6.00 x 2.00 m) with 6 piles 1.50 m in diameter. The pile caps were flush with the wing walls and protruded 2.00 m beyond the front walls. The pier foundations were 6.00 x 6.00 x 2.00 m pile caps with 4 piles 1.50 m in diameter. Figure 7 represents the structure described above.

The piers were modeled with 1.00 x 1.00 m shell elements similar to those used on the deck. The pier cap was modeled with the same type of element and its mesh was adjusted so that the nodes would coincide with the deck above. The foundations of the piers were modeled with 1 m 8-node solid hexahedral elements based on the standard isoparametric formulation. For the pier-footing connection, the two bottom layers of nodes in the piers were rigidly coupled with three rows of nodes on the surface of the footing. This implied that they all moved as a rigid body, which modeled the embedding of
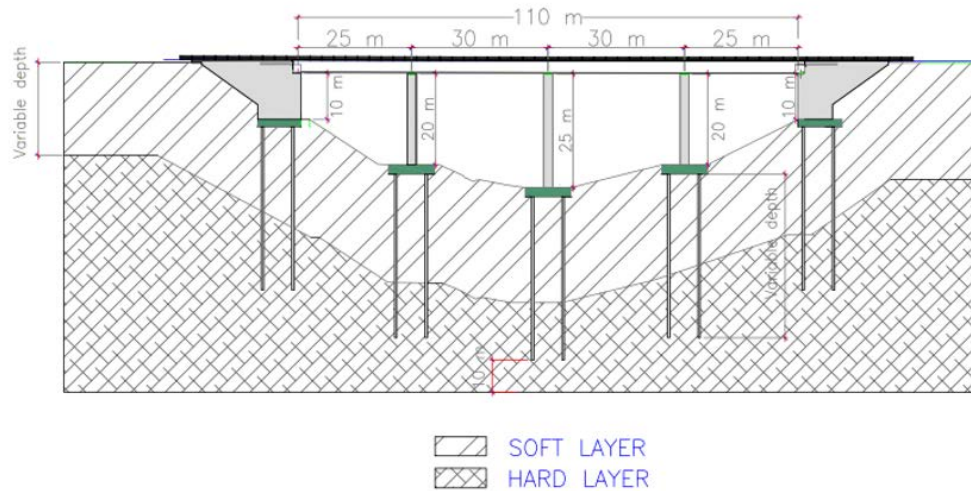
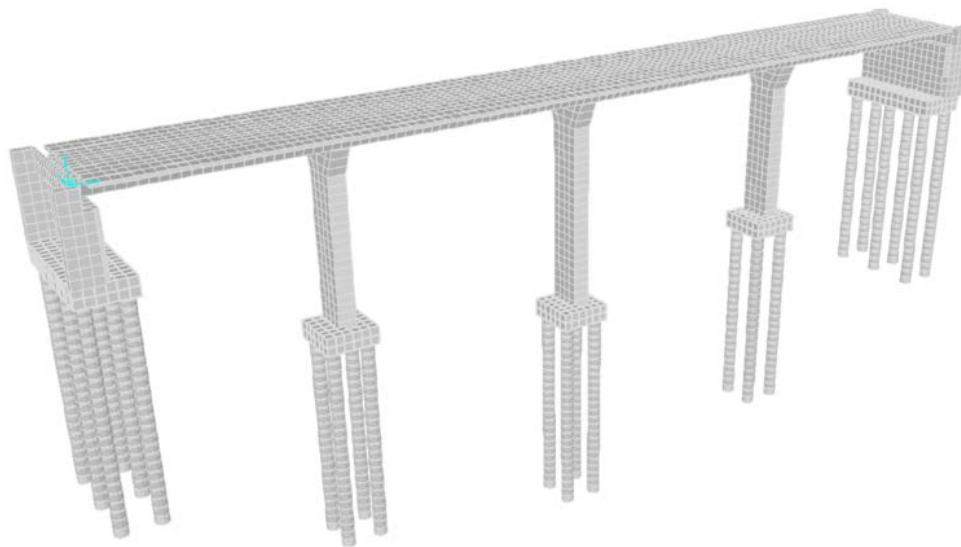Figure. 7. Longitudinal section of the complete model.

Figure. 8. Complete model discretization without soil.

the pier in the footing while allowing strains in the surrounding area. The abutments were also discretized in a similar way, with shell elements in the walls and solid elements in the foundations. Everything described above is shown in Figure 8.

A peculiarity of the abutments was that the soil inside them, specifically that contained between the wing walls and the back face of the front one, was included in the model as a solid element and matched the abutment element size. Thus, the overall stiffness and inertia of the system was better captured since it included the interaction with the backfill soil. The complete model also included the soil around the abutment and around the pile caps and piles. The model was extended with an additional 14 m of discretized soil around the foundation for a global model width of 34 m since the pile caps were 6 m wide (6 + 2 x 14). The soil depth of the soil included was 10 m greater than the deepest pile (i.e., middle pier foundation). The volume of soil included in these models was chosen in accordance with the results presented in Section 3.1.2.

Regarding soil stiffness, two different layers were considered: a soft layer, whose thickness and stiffness were variables to be ex-

plored, and a hard layer underneath, which extended 10 m below the deepest pile. The piles were always embedded 10 m within the stiffer material, whose mechanical properties were constant through the study. The pile caps are also embedded in the top layer and were 2 m high. Normal displacements were constrained on the soil boundary faces. A summary of the models analyzed is presented in Table 2 using Figure 9 to illustrate one of them.

TABLE 2.
Complete model dimensions

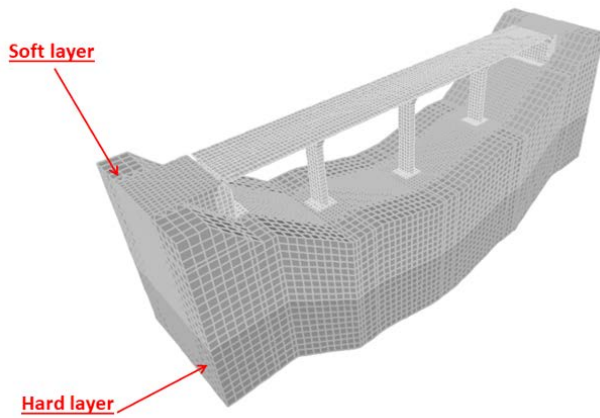| Soft layer depth (m)	Hard layer depth (m)	Pile foundation (m)	Modeled soil Depth (m)
4	20	12	24
6	20	14	26
8	20	16	28
10	20	18	30
12	20	20	32
14	20	22	34
16	20	24	36

Figure. 9. Complete model discretization.

Multiple analyses using different soil stiffness were performed to verify the importance of including the soil substructure while modeling deep foundation structures when considering their dynamic behavior. These stiffnesses were related to the wave propagation velocity (C_s, C_p, C_r) through the equations that govern the behavior of homogeneous isotropic materials, whose derivation can be found in Yang & Hung (2209) [40]. To estimate the stiffness of the terrain, the shear wave velocity (C_s) was used following the values and criteria proposed by seismic regulations.

For the hard layer material (i.e., the bottom one), a shear wave velocity of 800 m/s was used, corresponding to a material with a Young's modulus of 3,500 MPa, which remained unchanged throughout the studies. This corresponds to Type I ground (compact rock) according to the NSCP-07 [41], Type A ground (rock or other rock-like geological formation) in the Eurocode 8 [42] and Type B ground (i.e., rock) in the ASCE-7 [43]. For the soft layer material, three different stiffness levels were analyzed for all the depths listed in Table 2 (4, 6, 8, 10, 12, 14 and 16 m). Table 3 shows the mechanical properties of the selected soft layer material options next to their description or classification according to the different codes.

TABLE 3.
Soft layer material properties and classifications

C_s (m/s)	E (MPa)	NCSP-07	EC-8	ASCE 7
100	55	IV Soft cohesive soil	D Loose to medium cohesionless soil	E Soft Clay soil
300	500	III Average compactness	C Dense sand	D Stiff soil
575	1800	II Fracture rock	B Very dense sand	C Very dense soil

3.
RESULTS AND DISCUSSIONS

3.1. Simplified foundation model

The dynamic behavior of the simplified foundation models, as influenced by various parameters, was analyzed. Subsequently, complete models were constructed based on these findings.

3.1.1. Finite element size

Before considering the influence of element size, the effect of the meshing technique (i.e., pattern) on the results was analyzed. To this end, the displacement response at the center of the bottom face of the pile cap—when subjected to a short pulse (10 ms and 10 MPa)—was compared in the smallest foundation model variant (19.5 × 19.5 × 23.5) using two different mesh configurations. The first one – uniform mesh – had elements of similar dimensions throughout the domain (50 cm); the second one – locally refined mesh – had elements that increased in size in the soil when moving away from the foundation, from 50 cm at the interface with the foundation to 250 cm in the model outer contour. Figure 10 shows a comparison of these two meshing alternatives.

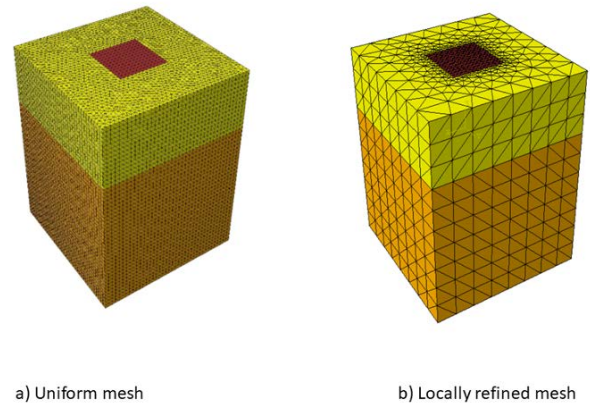

a) Uniform mesh   b) Locally refined mesh

Figure 10. Meshing technique comparison: uniform mesh (a) and locally refined mesh (b).

As shown in Figure 11, both meshing techniques yielded similar results. Therefore, the foundation dynamic behavior appeared to be insensitive to the meshing technique for this particular application. The mesh sizes and seeding techniques explored did not have a meaningful impact on the response of interest. The results obtained were effectively the same both for the uniform mesh model (Figure 10 a) and the locally refined mesh (Figure 10 b). Therefore, the locally refined mesh was chosen to minimize computational cost.
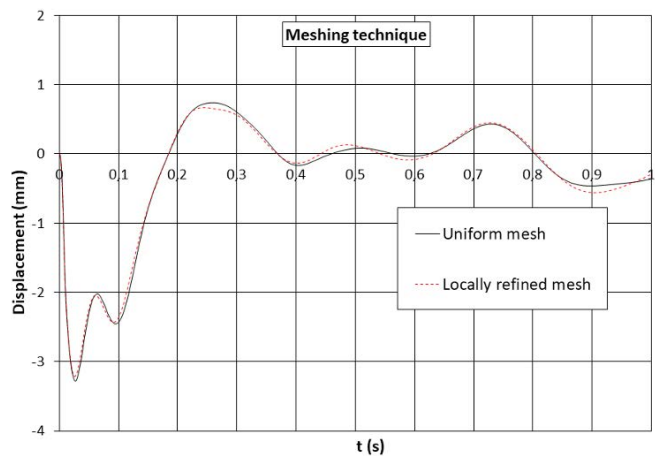

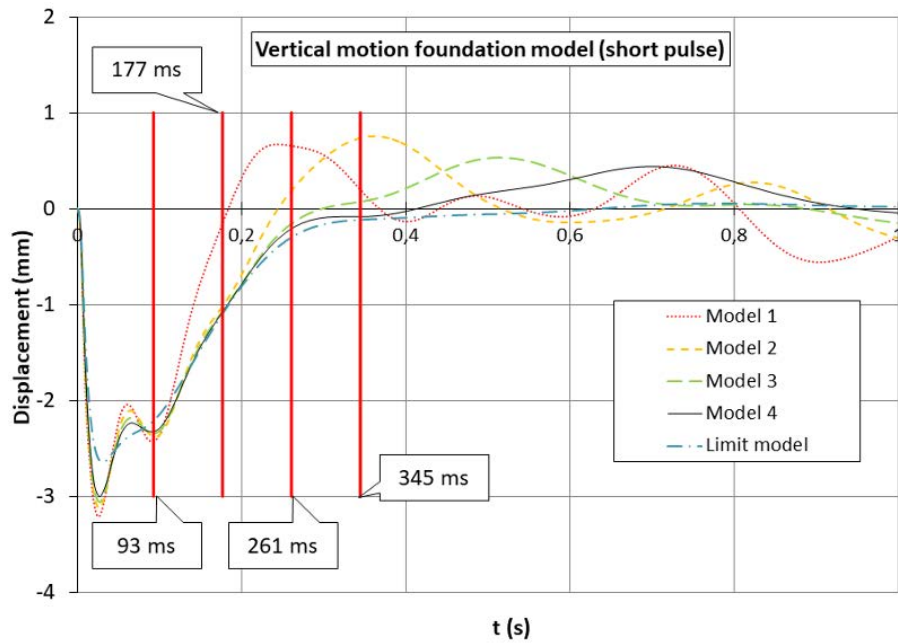Figure. 11. Results of the comparison of different mesh techniques in the simplified foundation model.

Figure 12. Terrain size response comparison under a 10 ms pulse (short pulse).
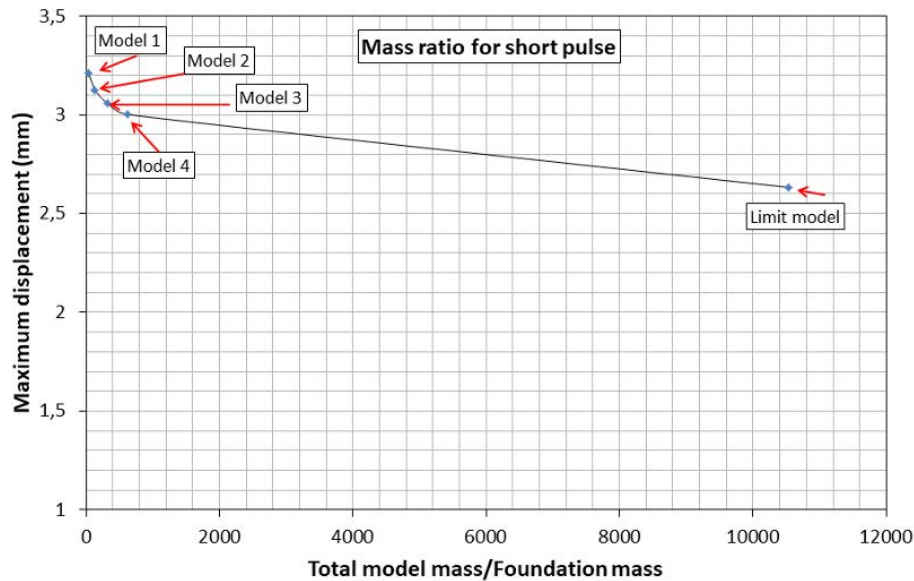

Figure 13. Maximum vertical displacements in the footing center for different total mass to footing mass ratios (short pulse).

Using the locally refined mesh technique, three element sizes were tested in the foundation, pile cap and piles: 30 cm, 40 cm and 50 cm, obtaining the following maximum displacement results (Table 4). The seeding on the soil outer boundary was kept at 250 cm across all models.

TABLE 4.

Maximum displacement for different element sizes

Element size (cm)	Maximum displacement (mm)
30	3.226
40	3.203
50	3.180

Similarly, for the locally refined models, the mesh refinement in the foundation, which ranged between 30 and 50 cm, did not affect the measured response either (Table 4). Consequently, a refined mesh of 50 cm in the interface was selected for the following studies with simplified foundations.

3.1.2. Influence of pulse duration and the amount of soil included

The response to a pulse of 10 ms (i.e., short pulse) was studied in the four models where the pile cap was surrounded by one, two, three or four times its dimension in soil (Table 1). In addition, a much larger model (162.5 x 162.5 x 95) was studied (Limit model). The vertical motion at the center of the bottom face of the pile cap is represented in Figure 12.
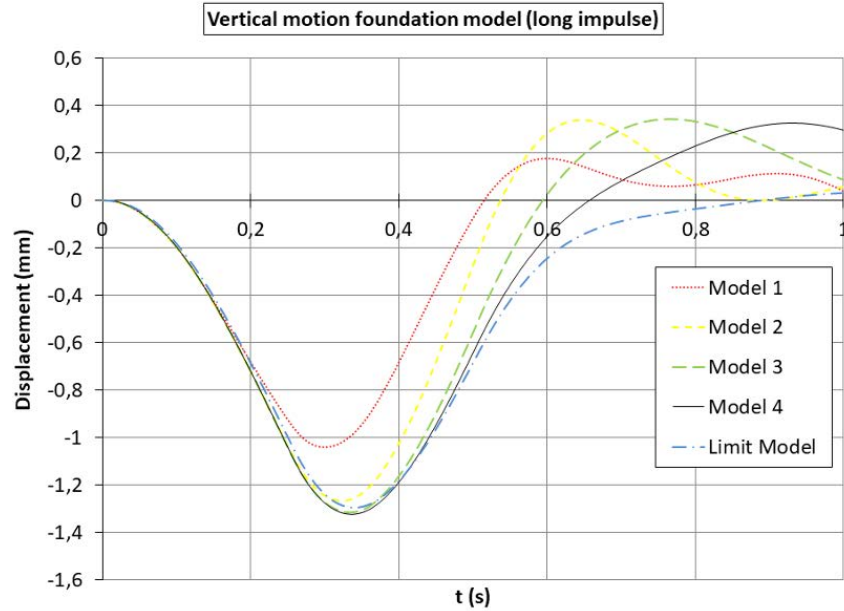
Figure. 14. Terrain size response comparison under a 500 ms pulse (long pulse).
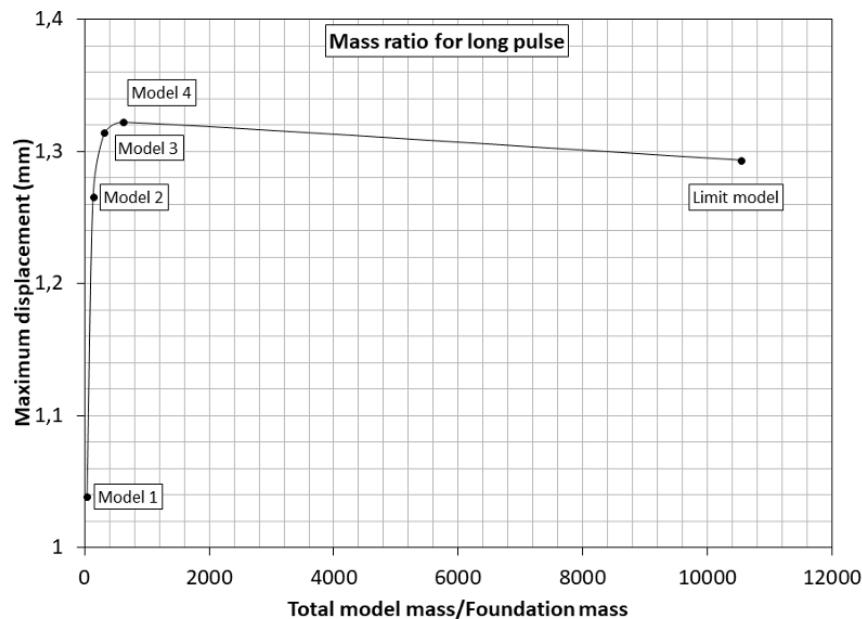

Figure 15. Maximum vertical displacements in the footing center for different total mass to footing mass ratios (long pulse).

¡A sudden settlement in the pile cap was observed immediately after the pulse, with a peak value that was very similar across models and that occurred approximately at 30 ms. After this first settlement, there was a high frequency oscillation that could not be due to the reflection of waves in the boundary since it occurred at the same time in all models. If it were due to the boundary wave reflection, the oscillation would be delayed by the increasing distance to the boundary.

In addition, the curves in Figure 12 diverged from the Limit model solution when the wave front, which had reached the boundary and bounced back, returned to the pile cap (93 ms, 177 ms, 261 ms, 345 ms). This high frequency oscillation that occurred at around 60 ms was indeed associated with the longitudinal vibration that occurs in the piles themselves. This

can be proven by increasing the mass of the piles making the phenomenon disappear (not shown in this research).

Figure 13 shows the maximum vertical displacement in the center of the footing against the ratio between the total model mass and the foundation mass. The solution converged with mass ratios over 600. This result was higher than the previous data obtained in shallow foundation models [20], where good results were obtained with a mass ratio in the order of 100. This showed a relevant difference between shallow foundations and deep foundations for a short pulse.

It is important to highlight that the excitation trains actually produce on the foundations of structures has a lower frequency content than the one analyzed so far. For this reason, the previous analysis was reproduced with a longer duration
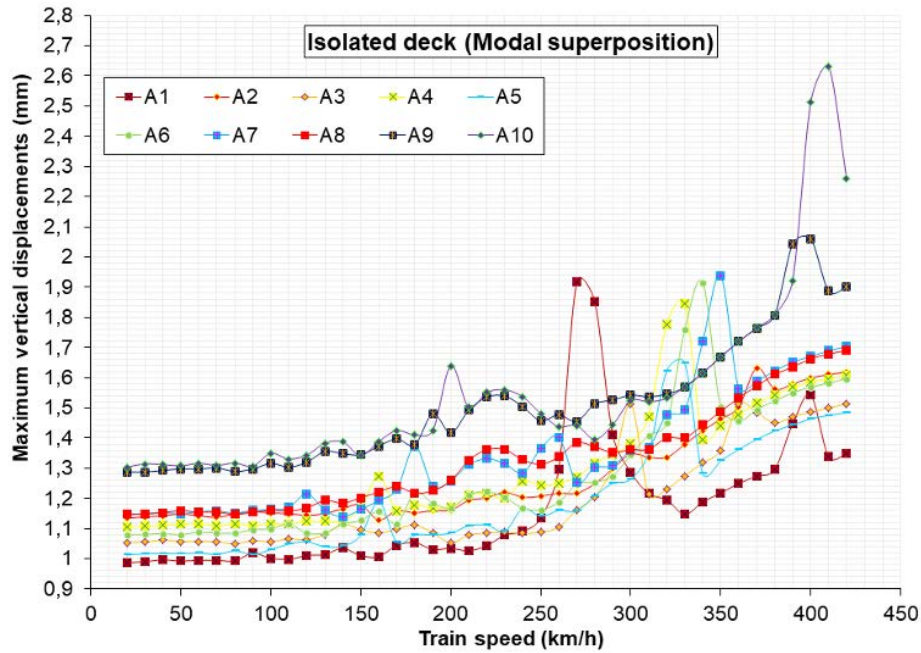
Figure. 16. Maximum vertical displacements in the isolated deck model (100 modes).

pulse – 500 ms – and a lower pressure – 20 KPa. Figure 14 shows the results under this new loading condition where more coincidences were observed.

Figure 15 shows the peak response against the ratio of the masses included in the model for long pulse analysis. It was observed that the mass required to be included in the model was significantly smaller than that required for short pulse analysis. In fact, the difference in results between Model 2 (32.5 x 32.5 x 30 m) and Model 4 (162.5 x 162.5 x 95 m) was only 2.17%, with the second model mass being only 130 times the mass of the foundation. Nevertheless, based on the aforementioned analysis, it was still necessary to include more soil in the deep foundation models than it was in the shallow foundation models, which only required a 20 total mass to foundation mass ratio under lower frequency excitation [20]. For longer pulses, (i.e., those that characterize the loading on high-speed railway bridge foundations), results were less sensitive to the amount of soil included, requiring as little as 100 times the mass of the foundation (Figure 15).

3.2. Bridge model

3.2.1. Isolated deck

The objective of this analysis was to evaluate the impact factor with traditional boundary conditions. These results were used as a benchmark to be compared against results of models where the soil substructure was included in order to understand its influence on the impact factor. Importantly, the impact factor definition used in this paper does not follow that specified in some standards such as the IAPF [10]. In those standards, the normalizing static load produces higher deformations and consequently lower impact factors. Figure 16 represents the recorded maximum displacement of the depicted node in Section 2.2.1 in 10 km/h speed increments for every HSLM train history load.

Modal superposition was used to obtain these results. The first 100 modes were used and captured 90.24% of the mass participation ratio associated to the vertical degrees of freedom. Results did not show any appreciable response amplification until 270 km/h were reached in the A1 train. This matched the bridge first resonance speed for A1 trains: 272.23 km/h. The resonance speed was obtained by multiplying the mode frequency by the distance between bogies of a particular train [44]. This same behavior also occurred with the other trains at higher speeds. In particular, the A10 train doubled its static response at 410 km/h. Proença et al. (2011) explored the effect of the type of track on the dynamic behavior of a high-speed railway bridge with 4 spans, also obtaining the maximum displacement for the A10 train.

Additionally, it was also shown previously [20] that these types of structures are well represented using the first few modes with the superposition method. More specifically, only a 0.228% difference was measured when comparing the superposition solution to that of a fully integrated model with the Newmark method (Impact factor - modal superposition = 2.011 vs. Impact factor - direct integration = 2.016).

3.2.2. Complete model of the railway bridge

Modal superposition should be used when considering the computational cost associated with performing an analysis in a model that includes piers, abutments, soil, and deep foundations using direct integration methods is unreasonable due to the number of analyses that need to be performed (i.e., multiple trains at multiple speeds).

3.2.2.1. Analysis with the number of modes included in the modal superposition

A sensitivity analysis of the number of modes included in the modal superposition was performed considering 100, 200, 300, 400 and 500 modes. As the number of modes increased,
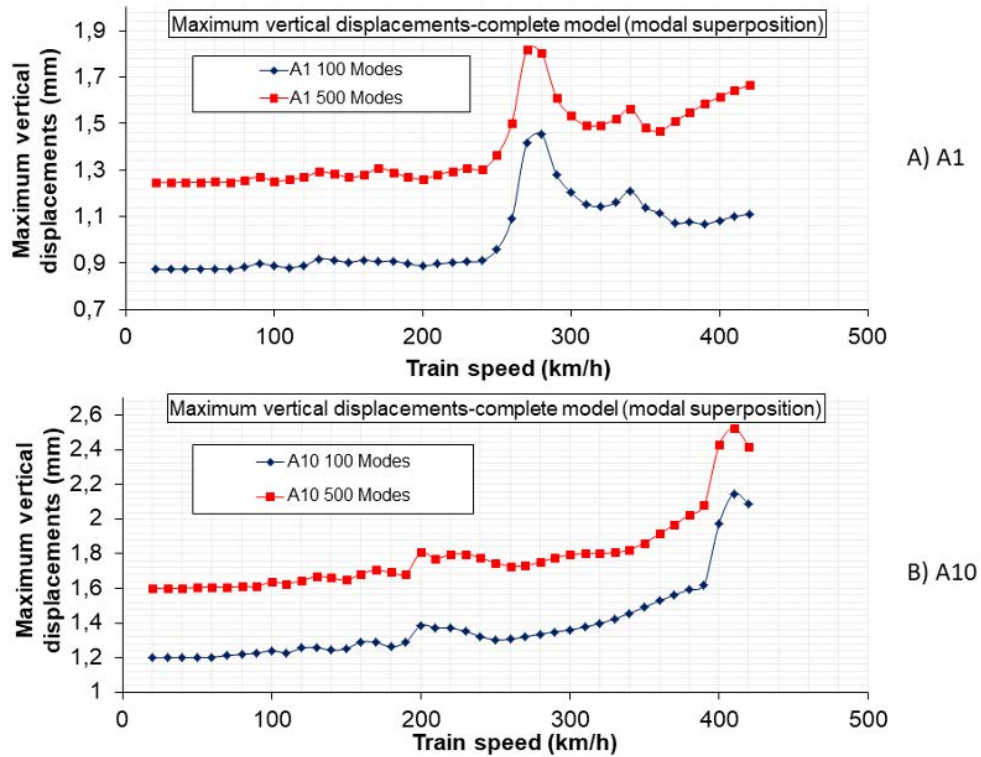
Figure 17. Maximum vertical displacements in the complete model (100-mode and 50-mode solutions for A1 and A10 trains).

the recorded maximum deflections also rose. Nevertheless, all the responses grew approximately proportionally across trains and speeds.

Figure 17 shows maximum displacement results obtained in models in which a 10 m soft layer of soil (C_s = 100 m/s) rests over a harder terrain (C_s = 750 m/s) for the A1 and A10 trains in the HSLM [9,10]. Maximum displacements for all the trains covered in the HSLM were computed but only A1 and A10 are represented for better readability of the results. As shown in Figure 17, the worst train-speed combination (A10 at 410 km/h) appeared to be independent of the number of modes included in the superposition analysis. The A10 train always exhibited a resonance at 410 km/h with a peak value that exceeded the maximum displacement for the A1 train and any other train in the HSLM at any speed, regardless of the number of modes included.

The maximum displacement increased with the number of modes included in the modal superposition solution without any sign of convergence, as observed in Figure 17. Consequently, the worst train-speed combination was rerun using direct integration to obtain accurate results. Given the results presented, it was decided to run the analysis sweeps in speeds and trains using modal superposition with 500 modes followed by a direct integration analysis of the worst-case model: the one with the train-speed combination that produced the highest displacements.

3.2.2.2. Soil stiffness sensitivity analysis

Figure 18 summarizes, for the train-speed combinations that produced the greatest displacements, the maximum vertical displacement for different soft layer material properties and depths. The maximum displacement for the isolated deck is also included for comparison. Please note that these are results obtained using direct integration in the worst cases identified through modal superposition.

When considering the effects of the soft layer material stiffness and depth (Figure 18) on the maximum displacement results, the response appeared to be insensitive to the depth of this superficial softer material layer but not to its stiffness. For the range of depths of soft material analyzed – 4 to 16 m – there was not a meaningful variation in the maximum displacement for a given layer stiffness, with all the results within 4% for each stiffness. However, the stiffness of this superficial layer played an important role in the final results, with higher maximum deflections when higher stiffness properties were used. This was the opposite of the effect on the static solution.

The train-speed combinations that produced the greatest displacements were 380, 390 and 410 km/h for A10 and A2 trains according to the HSLM classification used (Figure 18) [8]. The lack of trend in the speeds and type of train that produced the worst responses highlights the importance of exploring all types of trains used in the research and a wide range of speeds. Figure 19 shows, for the train-speed combinations that produced the greatest displacements, the maximum impact factor (Φ) for different soft layer material properties and depths. The impact factor for the isolated deck is also included for comparison.

When the results were analyzed in terms of the impact factor (Figure 19), which assesses dynamic amplification, the following was observed: response amplification depended very little on the soft layer depth but increased with its stiffness. This helps to understand why maximum displacement
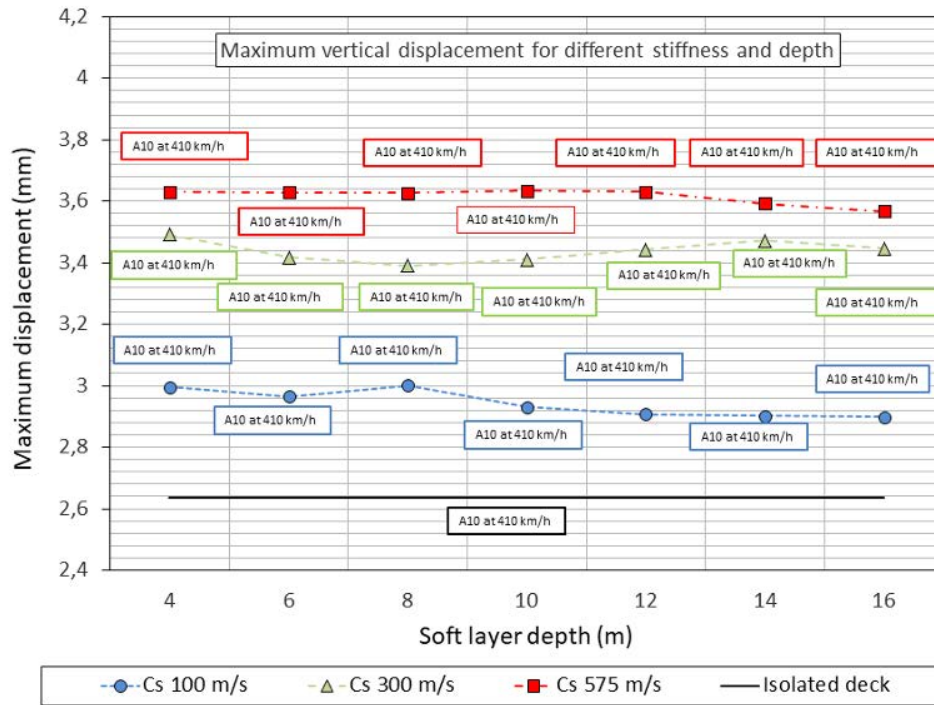
Figure 18. Maximum vertical displacements for different soft layer material stiffness and depth.
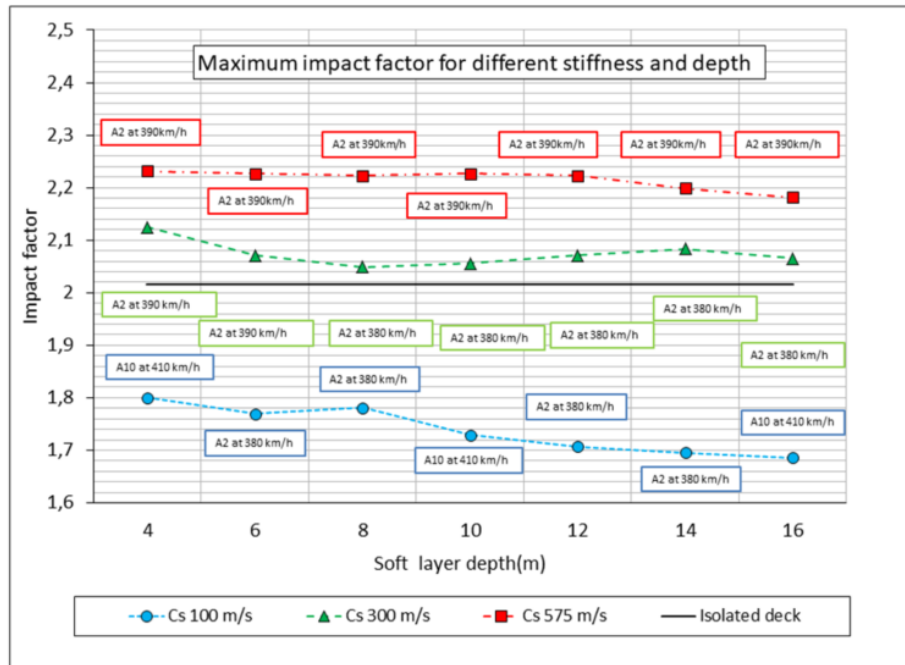

Figure 19. Maximum impact factor for different soft layer material stiffness and depth.

grows with soil stiffness. Even though a stiffer superficial layer slightly decreased the static deflection, the effect of stiffness on the impact factor coefficient was so important that it dominated the resulting dynamic maximum deflections.

When comparing these results with the benchmark – results of the isolated deck model – the maximum displacements of the isolated deck were even lower than the softer soft layer models. The impact factor coefficient lies somewhere between the different stiffness levels used for the soft layer. In other words, the isolated deck did not follow the trend defined by the stiffness of the soft layer material. To understand this, please note that, for an infinitely stiff soft layer material, the model analyzed would still include deformable piers and abutments. This conclusion could also be reached using stiffer soil models, but those models would not be realistic because they would not require deep foundations. This highlights the importance of including not only the surrounding terrain but also the main infrastructure (i.e., piers and abutments) in the model.

4.
CONCLUSIONS

The aim of the manuscript was to compare the results of the dynamic impact coefficient of a model without any infrastructure (i.e., isolated deck) with those of a model that included infrastructure (i.e., complete model). The research was conducted using the finite element method. First, the effect of model parameters (i.e., element size, pulse duration and volume of soil included in the model) was studied in a simplified foundation model.

Based on the results, some complete models were built with different variables: soil stiffness and depth, depth of the piles and a speed sweep from 20 km/h to 420 km/h, using 10 trains with different wheelbases and loads per axle. The following conclusions can be drawn from the simplified foundation models:

1. In this study, mesh sizes and seeding techniques did not have a meaningful impact on the response. Results showed convergence with a finite element size of 50 cm, regardless of the type of mesh used.
2. For a short pulse, associated to higher frequency events, significant differences were observed in the maximum displacements with the amount of soil included. In this case, a mass ratio of about 600 is recommended between total model mass and foundation mass.
3. For longer pulses, such as those that characterize the loading on high-speed railway bridge foundations, results were less sensitive to the amount of soil included. A total mass/foundation mass ratio of 100 was enough.
4. We found a relevant difference between shallow foundations and deep foundations.

In addition, the following conclusions can be drawn from the bridge models:

1. There were no differences (regarding the impact factor) between using modal superposition or direct integration for an isolated deck (Impact factor – modal superposition = 2.011 vs. Impact factor – direct integration = 2.016)
2. The sensitivity analysis to the number of modes included in the modal superposition for the complete model indicated that, as the number of modes increased, the recorded maximum deflections also rose.
3. To be more efficient (i.e., reduce computational cost), it is recommended to run the analysis sweeps in speeds and trains using modal superposition with 500 modes followed by a direct integration analysis of the worst case model (which produces the highest displacements).
4. The maximum displacement results were insensitive to the depth of the superficial softer material considered in the complete model.
5. The changes in the maximum displacement with the stiffness of the superficial layer played an important role in the final results. With the highest stiffness for this superficial layer (E=1800 MPa), the maximum displacement was 27.28% higher than in the isolated deck.
6. The dynamic response amplification (i.e., impact factor) depended very little on the soft layer depth but increased with its stiffness.
7. The isolated deck did not follow the trend defined by the stiffness of the soft material. To understand this, please note how, with an infinitely stiff soft layer material, the analyzed model would still include deformable piers and abutments.
8. The previous conclusion highlights the importance of including not only the surrounding terrain but also the main substructure (i.e., piers and abutments) in the model.

References

[1] G. Diana, Dynamic interaction of railway systems with large bridges, Vehicle System Dynamics 18 (1989) 71–106. https://doi.org/10.1080/00423118908968915.

[2] Ladislav. Frýba, Vibration of solids and structures under moving loads, Springer Netherlands, 1999.

[3] M. Klasztorny, Vertical vibrations of a multi-span beam steel bridge induced by a superfast passenger train, Structural Engineering and Mechanics 12 (2001) 267–281. https://doi.org/10.12989/sem.2001.12.3.267.

[4] H. Xia, N. Zhang, G. De Roeck, Dynamic analysis of high speed railway bridge under articulated trains, 81 (2003) 2467–2478. https://doi.org/10.1016/S0045-7949(03)00309-2.

[5] M. Shamsi, A. Ghanbari, Nonlinear dynamic analysis of Qom Monorail Bridge considering Soil-Pile-Bridge-Train Interaction, Transportation Geotechnics 22 (2020) 100309. https://doi.org/10.1016/j.trgeo.2019.100309.

[6] J. Shen-Haw, Resonance characteristics of high-speed trains passing simply supported bridges, J Sound Vib 267 (2003) 1127–41.

[7] C. Johansson, C. Pacoste, R. Karoumi, Closed-form solution for the mode superposition analysis of the vibration in multi-span beam bridges caused by concentrated moving loads, Comput Struct 119 (2013) 85–94. https://doi.org/10.1016/j.compstruc.2013.01.003.

[8] ERRI D214, Rail bridges for speeds > 200 Km/h. Final report. Part A: Synthesis of the results od D214 research, European Rail Research Institute, 1999.

[9] E. 1998-1 CEN, Eurocode 1: Actions on Structures-Part 2 : Traffic Loads on Bridges, (2003).

[10] Ministerio de Fomento, Code for actions for the Design of Railway Bridges, (2010).

[11] C. Svedholm, Efficient Modelling Techniques for Vibration Analyses of Railway Bridges, (2017) 1–90.

[12] C. Johansson, N.Á.N. Nualláin, C. Pacoste, A. Andersson, A methodology for the preliminary assessment of existing railway bridges for high-speed traffic, Eng Struct 58 (2014) 25–35. https://doi.org/10.1016/j.engstruct.2013.10.011.

[13] J.M. Goicolea, F. Gabaldón, F. Riquelme, Design Issues for Dynamics of High Speed Railway Bridges, Dynamics of High-Speed Railway Bridges (2005).

[14] M. Majka, M. Hartnett, Effects of speed, load and damping on the dynamic response of railway bridges and vehicles, Comput Struct 86 (2008) 556–572. https://doi.org/10.1016/j.compstruc.2007.05.002.

[15] S.G.M. Neves, A direct method for analyzing the vertical vehicle-structure interaction, Eng Struct 34 (2012) 414–420. https://doi.org/10.1016/j.engstruct.2011.10.010.

[16] K. Knothe, S.L. Grassie, Modelling of Railway Track and Vehicle/Track Interaction at High Frequencies, 1993. https://doi.org/10.1080/00423119308969027.

[17] E.Esmailzadeh, Vehicle–passenger–structure interaction of uniform bridges traversed by moving vehicles, J Sound Vib 260(4) (2003) 611–635.

[18] Y.B.Q.P. Hongye Gou; Chang Liu; Hui Hua, Mapping relationship between dynamic responses of high-speed trains and additional bridge deformations, (2020). https://doi.org/https://doi.org/10.1177/1077546320936899.

[19] M. Szafrański, A dynamic vehicle-bridge model based on the modal identification results of an existing EN57 train and bridge spans with non-ballasted tracks, Mech Syst Signal Process 146 (2021). https://doi.org/10.1016/j.ymssp.2020.107039.

[20] A. Martínez-De la Concha, H. Cifuentes, F. Medina, A Finite Element Methodology to Study Soil–Structure Interaction in High-Speed Railway Bridges, J Comput Nonlinear Dyn 13 (2018) 031010. https://doi.org/10.1115/1.4038819.

[21] H. Li, Z. Yu, J. Mao, L. Jiang, Nonlinear random seismic analysis of 3D high-speed railway track-bridge system based on OpenSEES, Structures 24 (2020) 87–98. https://doi.org/10.1016/j.istruc.2020.01.003.

[22] A. Zangeneh, A. Andersson, C. Pacoste, Identification of soil-structure interaction effect in a portal frame railway bridge through full-scale dynamic testing, 159 (2018) 299–309. https://doi.org/10.1016/j.engstruct.2018.01.014.

[23] B. Takemiya, Shinkansen high-speed train induced ground vibrations in view of viaduct–ground interaction, Soil Dynamics and Earthquake Engineering 27(6) (2007) 506–20.

[24] M. Ülker-Kaustell, R. Karoumi, C. Pacoste, Simplified analysis of the dynamic soil-structure interaction of a portal frame railway bridge, Eng Struct 32 (2010) 3692–3698. https://doi.org/10.1016/j.engstruct.2010.08.013.

[25] J. Vega, A. Fraile, E. Alarcon, L. Hermanns, Dynamic response of underpasses for high-speed train lines, J Sound Vib 331 (2012) 5125–5140. https://doi.org/10.1016/j.jsv.2012.07.005.

[26] A. Zangeneh, C. Svedholm, A. Andersson, C. Pacoste, R. Karoumi, Dynamic Stiffness Identification of Portal Frame Bridge – Soil System using Controlled Dynamic Testing, Procedia Eng 199 (2017) 1062–1067. https://doi.org/10.1016/j.proeng.2017.09.293.

[27] A. Romero, M. Solís, J. Domínguez, P. Galvín, Soil-structure interaction in resonant railway bridges, Soil Dynamics and Earthquake Engineering 47 (2013) 108–116. https://doi.org/10.1016/j.soildyn.2012.07.014.

[28] A. Doménech, M.D. Martínez-Rodrigo, A. Romero, P. Galvín, Soil–structure interaction effects on the resonant response of railway bridges under high-speed traffic, International Journal of Rail Transportation 3 (2015) 201–214. https://doi.org/10.1080/23248378.2015.1076621.

[29] J. Domínguez, J. Roesset, Dynamic stiffness of rectangular foundations, MIT Research Report R Cambridge (1978).

[30] S.-H. Kim, M. Shinozuka, Development of fragility curves of bridges retrofitted by column jacketing, Probabilistic Engineering Mechanics 19 (2004) 105–112. https://doi.org/10.1016/j.probengmech.2003.11.009.

[31] J.-W. Lin, C.-W. Chen, S.-H. Chung, Modeling and assessment of bridge structure for seismic hazard prevention, Natural Hazards 61 (2011) 1115–1126. https://doi.org/10.1007/s11069-011-9969-3.

[32] K.-J. Bathe, Finite Element Procedures, Prentice Hall, 1996.

[33] A. Martínez-de la Concha, J.D. Ríos, H. Cifuentes, Numerical Study of the Shear Behavior of Ultra-High-Performance Concrete Beams, Hormigon y Acero 75 (2024) 157–162. https://doi.org/10.33586/hya.2023.3119.

[34] L. Cañizo, B. Escario, C. Faraco, L. Fort, J.A. Jiménez Salas, J.L. Justo Alpañés, M. Llorens, C. Lorente de No, R. Marsal, R. Molina, F. Muzas, C. Oteo, J.M. Rodríguez Ortiz, M. Romana, A. Serrano, A. Soriano, A. Uriel, S. Uriel, Geotecnia y cimientos, Servicio de Publicaciones de alumnos, Madrid, 1970.

[35] Ministerio de Fomento, Norma de Construcción Sismorresistente : Puentes (NCSP-07), (2008).

[36] L. Frýba, Traffic loads on railway bridges, Dynamics of Railway Bridges (1996) 183–198. https://doi.org/10.1680/dorb.34716.0010.

[37] A. Romero, P. Galvín, J. Domínguez, Comportamiento dinámico de viaductos cortos considerando la interacción vehículo-vía-estructura-suelo, Revista Internacional Para Metodos Numericos Para Calculo y Diseno En Ingenieria 28 (2012) 55–63. https://doi.org/10.1016/j.rimni.2011.11.004.

[38] M.D. Martínez-Rodrigo, Atenuación de vibraciones resonantes en puentes de ferrocarril de Alta Velocidad mediante amortiguadores fluido-viscosos, (2009). https://doi.org/10.1200/JCO.2009.26.8789.

[39] ADIF, IGP-5 Instructions and recommendations on Spanish Railway Structures, (2011).

[40] Y.B. Yang, H.H. Hung, Wave Propagation for Train-Induced Vibrations, World Scientific, 2009.

[41] Ministerio de Fomento, Norma de Construcción Sismorresistente : Puentes (NCSP-07), (2008).

[42] CEN, EN 1998-1: Eurocode 8 Design of structures for earthquake resistance. Part 1 : General rules, seismic actions and rules for buildings, (2011).

[43] Asce/Sei, Minimum design loads for buildings and other structures, ASCE Standard (2010) 608. https://doi.org/10.1061/9780784412916.

[44] B.H. Kim, J. Lee, D.H. Lee, Extracting modal parameters of high-speed railway bridge using the TDD technique, Mech Syst Signal Process 24 (2010) 707–720. https://doi.org/10.1016/j.ymssp.2009.11.010.

[45] J.M. Proença, H. Casal, M. Neves, Effect of the type of track on the dynamic behaviour of high speed railway brigdes, 3rd International Conference on Computational Methods in Structural Dynamics and Earthquake Engineering: An IACM Special Interest Conference, Programme (2011) 25–28.